JOURNAL OF THEORETICAL
AND APPLIED MECHANICS
https://doi.org/10.15632/jtam-pl/207298
ONLINE FIRST

IMPACT ACCELERATION ACQUISITION WITH A HIGH FREQUENCY DATA LOGGING SYSTEM BASED ON SPI COMMUNICATION PROTOCOL

Kamil KURPANIK, Jonasz HARTWICH, Sławomir KCIUK, Sławomir DUDA

Faculty of Mechanical Engineering Technology, Silesian University of Technology, Gliwice, Poland
*corresponding author, *kamil.kurpanik@polsl.pl*

As part of the research conducted, the correctness of the serial peripheral interface (SPI) communication was tested using the Raspberry Pi 4B. The purpose of the experiment was to confirm the possibility of stable data exchange between the control unit and external peripheral circuits, with particular emphasis on analog-to-digital converters and micro-electro-mechanical systems (MEMS) sensors. The tests showed correct and stable operation of the SPI bus for both unidirectional and bidirectional transmission, and confirmed the usefulness of SPI in measurement systems requiring precise and fast data transfer. The experiments provide a basis for further work with real-time sensors and data acquisition systems under dynamic conditions.

Keywords: data logging system; MEMS; SPI; impact acceleration; high frequency.

1. Introduction

The recording of shock wave parameters is the basis of a significant amount of research aimed at improving the safety of military vehicle crews (Baranowski *et al.*, 2020; Pyka *et al.*, 2025). A significant parameter measured in such experiments is the acceleration, which can reach a value of several hundred g in less than a few milliseconds (Kciuk *et al.*, 2022). It is particularly important to register this parameter since the forces resulting from these accelerations through the impact of the vehicle's structure are transmitted directly to the crew, which can lead to death or serious injuries such as spinal cord fracture (Elsayed & Atkins, 2008). Measurements of rapidly changing acceleration values are also used in civilian industry, an example of this type of research is car crash tests (Dima & Covaciu, 2017; Olvey *et al.*, 2004). The recording of shock wave parameters also provides a reference for numerical simulations (Arkusz *et al.*, 2019; Erdik *et al.*, 2016; Wrazidło *et al.*, 2025).

The most commonly used sensors for acceleration measurements are devices based on micro-electro-mechanical systems (MEMS) technology. These are defined as minimized mechanical and electromechanical components (with dimensions of a few hundred micrometers at most) (Covaciu & Dima, 2017). An accelerometer is essentially a capacitive or piezoresistive device consisting of a suspended pendulum proof mass/plate assembly. In the case of capacitive accelerometers, the displacement of the test mass induces a change in capacitance of the capacitor, allowing the determination of acceleration (Sethuramalingam & Vimalajuliet, 2010). The primary parameters

Ministry of Science and Higher Education
Republic of Poland

This publication has been funded by the Polish Ministry of Science and Higher Education under the Excellent Science II programme "Support for scientific conferences".
The content of this article was presented during the 61st Symposium "Modelowanie w mechanice" (Modelling in Mechanics), Szczyrk, Poland, March 2–5, 2025.

that define the applicability of a given accelerometer within a specific application are the output range and measurement resolution. Nonetheless, in the context of research investigating the impact of shock waves on human health, two crucial factors must be given due consideration. Firstly, the frequency bandwidth carried by the sensor and, secondly, the sampling frequency of the entire measurement system. In order to record a peak of acceleration values lasting only a few milliseconds during the measurement process, the sampling frequency must be sufficiently high. In the process of designing the measurement system, particular attention must be paid to the digitization of the voltage signal from the MEMS-type sensor, as well as to the communication protocols.

The signal from the MEMS-type accelerometer after sampling must be sent to the data logger, which can be devices such as microcontroller, microcomputer, etc. In the issue of recording the acceleration during the passage of the shock wave, the speed of data transmission is very important to avoid loss of measurement data. An example of a communication interface that is straightforward to implement and possible to use in the issue under consideration is the serial peripheral interface (SPI). This interface is most often used for systems requiring low and medium data transfer rates (Anand *et al.*, 2014), but can also be successfully used in systems requiring higher communication speeds (Brezeanu *et al.*, 2022; Coşkun *et al.*, 2023; Mohd Noor & Saparon, 2012). An important element of the communication system that needs to be considered is also the distance over which the communication is carried out. In contrast to long-distance communication protocols such as USB (Universal Serial Bus), PCI (Peripheral Component Interconnect), and Ethernet (Park & Mackay, 2003), SPI along with interfaces such as I2C (Inter-Integrated Circuits) and CAN (Control Area Network), is commonly used for short and medium-distance communication. In the issue of recording shock wave parameters, long-distance communication is most often required for safety reasons, which involves signal conditioning, especially for low-voltage signals like those from MEMS-type accelerometers. Signal conditioning is associated with an increase in interference, so the use of communications like SPI with a properly protected data logger could be an improvement in this type of measurement. SPI, compared to other similar communication protocols, is characterized by high transmission rates combined with minimal hardware requirements (Vijaya *et al.*, 2011). SPI has a higher transmission speed than similar communication protocols like I2C and UART (Universal Asynchronous Receiver and Transmitter). In contrast to the semi-duplex nature of I2C, which utilizes a single data line (SDA) and a clock line (SCL), SPI facilitates full-duplex communication through the implementation of dedicated transmit (MOSI – Master Output Slave Input) and receive (MISO – Master Input Slave Output) lines. Conversely, UART, despite its simplicity and frequent utilization for point-to-point communication, also operates in half-duplex (or quasi full-duplex, depending on the implementation) mode and does not offer the ability to exchange data as quickly and simultaneously as SPI. In addition, SPI does not require device addressing like I2C, which simplifies the protocol and allows much higher transmission speeds (even tens of MHz), making it an ideal choice for systems requiring fast, reliable and synchronous communication with multiple devices.

The purpose of this paper is to verify the feasibility of using the SPI communication interface in the design of the authors' MEMS accelerometer-based shock wave feature recorder. The paper discusses technical issues related to the development of a communication interface designed for the problem at hand. Furthermore, a series of experiments has been conducted to ascertain the efficacy of the system under development. As part of this experimental research, a constant voltage was applied to the output of the analog to digital converter (ADC) in order to verify the correct discretization of the input signal and to evaluate the noise of the signal at sampling frequencies up to 45 kHz. In addition, as part of this paper, some comparative research of various measurement systems was carried out on the issue of recording data from dynamic phenomena. As part of this experiment, force and acceleration were measured during the impact of a hammer suspended on a pendulum against a bumper placed at the pendulum's equilibrium center. The conduction of this research enabled a comparison of the quality of recorded data from

different measurement systems, whilst also enabling preliminary verification of the possibility of uprooting the developed recorder based on the MEMS accelerometers in the research of dynamic phenomena. The developed measurement system demonstrates a less common approach to the research of shock wave characteristics, precisely by employing medium-distance communication that does not necessitate the conditioning of the measurement signal. In this approach, the data logger must be relatively close to the sensor, which means that it will be in the range of the shock wave and must be protected from its influence. Furthermore, the development of an original measurement system affords the authors greater autonomy in the development of the software utilized. It is important to note the potential for the utilization of neural networks, which are being employed with increasing frequency in sensory systems (Kciuk *et al.*, 2023), in addressing a particular issue. This involves the development of a model that can ascertain the impact of the wave on human health, with this model being based on the readings obtained from the data logger.

2. Method

The SPI communication interface used in this work operates in a master-slave configuration in half-duplex mode. The chip select (CS) line is responsible for initiating communication between devices. This communication is only active when the line is in a low state, and this state must be maintained for the duration of the communication. It has been established that an oscillating digital clock (DCLK) signal is shared between the Master and the Slave. This signal dictates the timing of bit transmission on the data line (Texas Instruments, 2010). The signal on the DCLK line is generated by the device that is in master communication. The transmission rate is directly related to the clock frequency, since one bit is transmitted only during a single clock cycle. This ensures coordinated data transfer (Lynch *et al.*, 2015) by informing the Master and Slave when to initiate communication. The digital input (DIN) and digital output (DOUT) lines are the data lines telling the Master to send a request to the Slave and sending a response from the Slave to the Master, respectively. Figure 1 shows a simplified diagram of the communication between the microcomputer and the ADC.

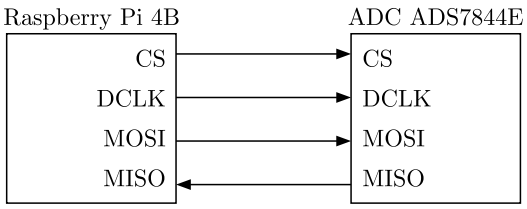

Fig. 1. Simplified diagram of the communication between the registrar (Raspberry Pi 4B) and the ADC.

With reference to the principles of the SPI interface discussed earlier and the characteristics of the transmitter used, the diagram in Fig. 2 shows a detailed sequence of data exchange between the microcontroller and the measurement system. The illustration shows the timing relationships between the basic signals of the SPI bus: DCLK, CS line (CS), input data line (MOSI), and output data line (MISO). Also indicated are the activation moments of the various transmission phases, including communication initialization, transmission of control commands and reading of measurement data. Analysis of this sequence allows fine-tuning of the microcontroller's configuration to meet the timing requirements of the transmitter, which is key to ensuring correct synchronization and reliability of data transmission. The detailed timing and communication scheme for SPI data exchange is shown in Fig. 2.

The measurement system used in the experiment consisted of the following components: Raspberry Pi 4B with Raspberry Pi OS (based on Debian) installed, acting as a control and data logging unit; ADS7844E analog-to-digital converter – a 12-bit, 8-channel chip communicating

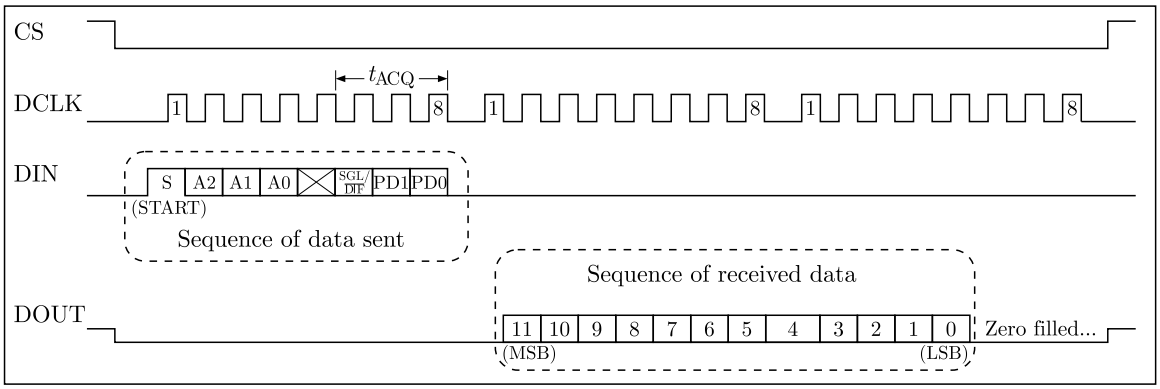

Fig. 2. SPI communication timing diagram as specified in the device datasheet, showing the sequential exchange of control and data bytes.

with the Raspberry Pi via the SPI interface; and a laboratory power supply generating a test voltage in the range of 0 V–3.3 V. The ADS7844E transducer was powered by 3.3 V, supplied by a voltage regulator that also served as the reference voltage source (Vref). SPI bus connections (DCLK, MISO, MOSI, and CS) were established in accordance with the ADS7844E's technical documentation and the Raspberry Pi 4B's GPIO pin layout.

The following waveform (Fig. 3) presents the outcome of measuring SPI communication in "every byte" transmission mode, which was recorded with a digital oscilloscope. Clearly defined sequences of clock pulses (DCLK) and data line activations (MOSI/MISO) can be seen, corresponding to single bytes transmitted in a single transaction. Significantly, the presence of minor interference and noise in the signal lines is observed, which appears only during inactive periods, i.e., between consecutive transmissions. This localization of interference clearly indicates that it is not generated by the MEMS chip itself or the transducer during operation, but is of an external nature (e.g., coming from the power supply, electromagnetic interference or reflections on the transmission lines). This confirms the correctness of the data exchange process itself, while at the same time emphasizing the need to address shielding issues.

Fig. 3. Oscilloscope capture of a single SPI data exchange sequence between the microcontroller and the MEMS sensor, illustrating the timing relationship between clock and data lines.

Figure 4 shows the course of communication in the mode of reading every second byte, used to filter irrelevant information selectively. In this variant, only those fragments of transmission that correspond to the relevant measurement data are received, while bits present outside the main exchange sequence are skipped. As a result, the recorded waveform is clearer, and only key moments related to the transmission of utility values are analyzed.

In order to reduce distortion and minimize the impact of noise on the measurement signal, the data acquisition process uses a strategy of receiving every second response from the SPI

Fig. 4. Oscilloscope capture of SPI communication in reduced sampling mode (every second byte), showing selective acquisition of relevant data segments.

system. The received data is then processed using a bit mask, taking into account the fact that the oldest bit (MSB) is transmitted first. If an interference occurs when the most significant bit is transmitted, the potential error is 50 % of the full measurement range. The designed algorithm effectively bypasses this kind of failure, providing transmission error robustness. In addition, the use of a bit mask makes it possible to correct the data already at the recording stage, which significantly increases the reliability of the system. Despite the simplified filtering procedure, the solution makes it possible to achieve a stable sampling frequency of 45 kHz, which is a significant advantage over piezoelectric sensor systems, which achieve about 20 kHz per channel. The algorithm for processing a single packet of data is presented in Fig. 5.

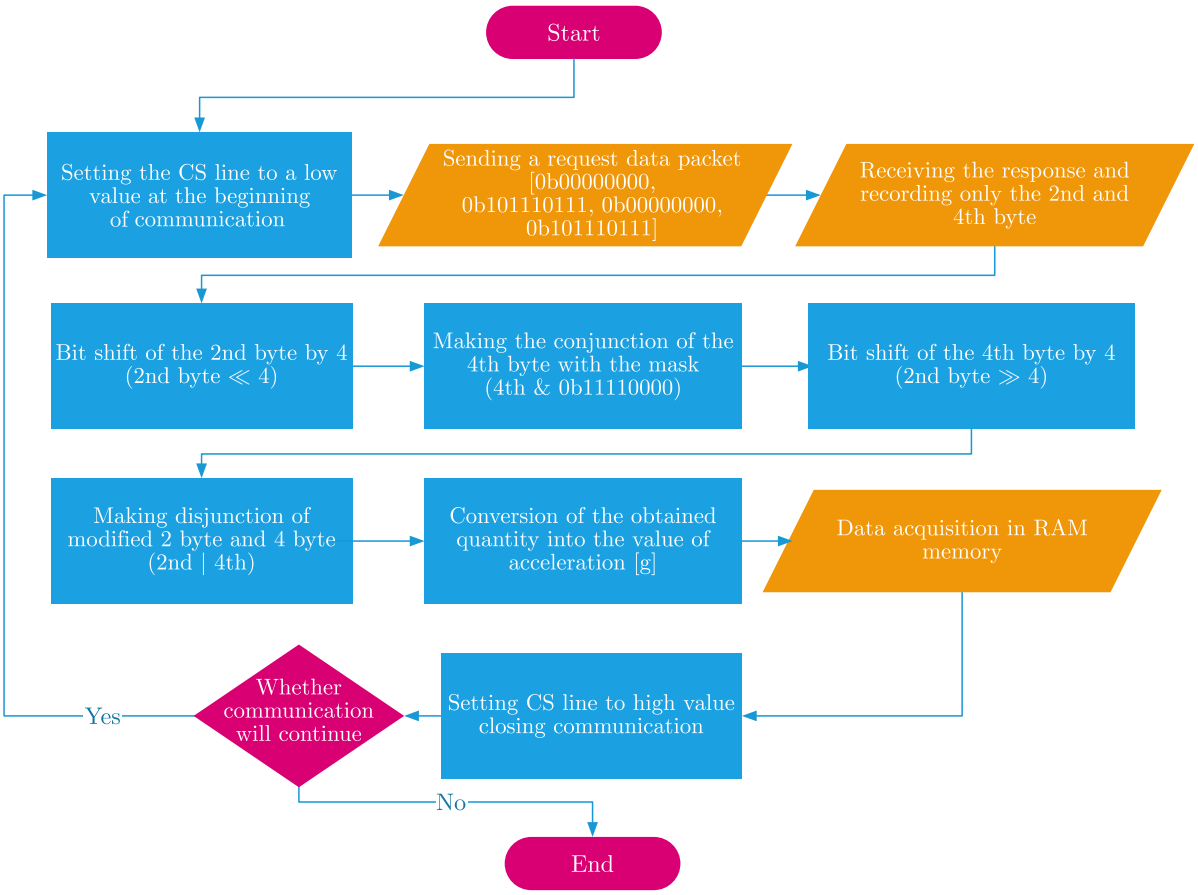

Fig. 5. Block diagram of the algorithm for data transmission, reception, and processing within the MEMS-based measurement system.

As a preliminary test, the DC voltage was measured from a bench power supply, applied to one of the analog inputs of the ADS7844E converter. The purpose of the test was to verify the correct operation of the entire measurement path and to evaluate the accuracy of the conversion of the analog signal to digital form. The output voltage from the power supply was set at several levels (0.6 V, 1.65 V, 2.4 V, 3.3 V) – including those corresponding to the power supply of the sensor used later in the project. Data reading from the transmitter was implemented using the Python language and the spidev library to handle the SPI bus. The raw digital values were scaled to the corresponding voltage values, and then compared with measurements taken in parallel using a multimeter to assess the accuracy of the transmitter.

Figure 6 shows the voltage readings measured by the ADS7844E converter. The readings from the converter show good agreement with the reference values, which confirms the correctness of the measurement path. The voltages are stable, and the differences were within the acceptable range of measurement error (oscillations due to power supply interference). The initial and final distortions seen in the graph are due to signal filtering effects associated with the limited sampling range and the operation of the smoothing algorithm. These results confirm that the circuit can be used for further measurements in the project.

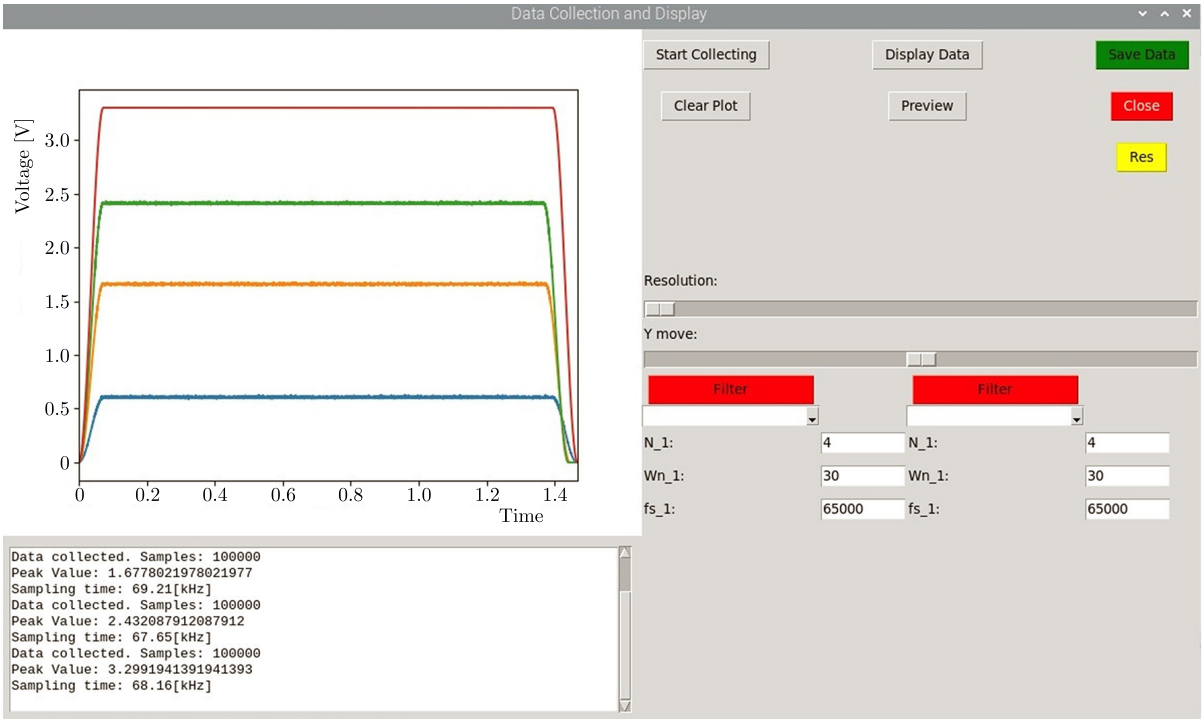

Fig. 6. Graphical user interface (GUI) screenshot illustrating the test of SPI communication between the ADC module and the microcomputer.

A physical pendulum is any rigid body that can make free oscillatory motions about a horizontal axis not passing through its center of mass, under the influence of gravity. Unlike the ideal mathematical pendulum – which is a model of a material point suspended from a weightless and inextensible thread – the physical pendulum takes into account the actual geometric properties and mass distribution of the body. In the experiment conducted, this system was used to generate a controlled force pulse by striking a force sensor with the tip of the pendulum. At the same time, the response of the measurement system based on a MEMS accelerometer integrated into a Raspberry Pi 4B microcomputer via an SPI interface was recorded. The results were compared with values obtained from a piezoelectric sensor system, built with independent acceleration sensors, to evaluate the accuracy and sensitivity of the MEMS system under dynamic forcing conditions.

During the experiment, the pendulum shown in Fig. 7 was released from two fixed angles of deflection: 20° and 40°. At the lowest point of the trajectory, contact was made between the tip of the pendulum and the FC500 force sensor (AXIS Sp. z o.o., Gdansk, Poland) (FC500), allowing precise measurement of the impact force. Simultaneous data recording was carried out from three independent measurement systems: the force sensor, a MEMS ADXL377 accelerometer (Analog Devices, USA) (ADXL377) connected to a Raspberry Pi 4B microcomputer via an SPI interface, and a piezoelectric sensor system – the MTS DSP SigLab 20-42 Dynamic Signal Analyzer (MTS Systems Corporation, USA) – consisting of PCB Piezotronics 333B31 (PCB Piezotronics, USA) (333B31) and 352C33 (PCB Piezotronics, USA) (352C33) acceleration sensors. Due to the temporal synchronization of all measurement channels, it was possible to compare the obtained results and assess their mutual compatibility directly. The purpose of the measurements was both to calibrate the SPI-based data acquisition system and to verify the quality of the MEMS accelerometer signal readout in the context of future applications for analyzing dynamic phenomena. For each of the two tilt angles, 30 independent measurements were made, ensuring the statistical reliability of the data obtained.

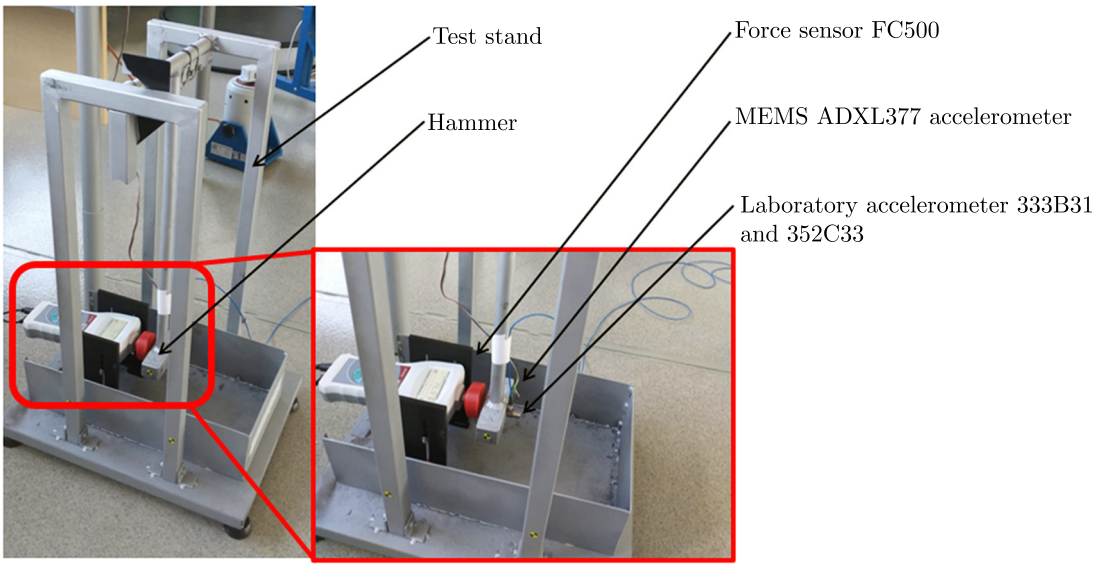

Fig. 7. Experimental setup with physical pendulum and mounted sensors, including a force sensor at the impact point, a MEMS accelerometer, and reference acceleration sensors. The MEMS unit is connected to a Raspberry Pi 4B for acquisition of dynamic response data via SPI interface.

3. Results and discussion

Experimental research was performed for two selected pendulum swing angles: 20° and 40°. In each case, the pendulum was released from a fixed angle and then struck a force sensor fixed at a fixed point. Based on the recorded signal from the sensor, the maximum value of the peak impact force was determined. At the same time, accelerations obtained from two independent sources were recorded: from a MEMS accelerometer integrated into a Raspberry Pi-based measurement system and from piezoelectric acceleration sensors, which are a separate measurement system (MTS DSP SigLab). The results of 30 consecutive impacts are summarized for the 20° and 40° deflection accounts in Table 1.

The lowest recorded spread of values over a period of 30 consecutive measurements has been documented for the FC500 force sensor, as evidenced by the coefficient of variation, which does not exceed 3 %. Additionally, the low spread of data is characterized by results recorded with the use of a logger, employing a MEMS capacitive accelerometer, for which the coefficient of variation does not exceed 5 %. Data recorded with the MEMS accelerometer is characterized by the

Table 1. Maximum values of the recorded force (FC500 force sensor) and acceleration (MEMS accelerometer, piezoelectric accelerometers 333B31 and 352C33) during 30 consecutive hammer impacts for the pendulum swing angle of 20° and 40°.

	FC500		MEMS		333B31		352C33	
Swing angle	20°	40°	20°	40°	20°	40°	20°	40°
	72.60	155.50	15.17	28.85	12.80	24.10	10.70	23.30
	75.30	156.50	14.39	28.46	12.70	23.80	10.40	23.80
	79.90	150.20	15.76	28.85	15.20	27.40	14.40	24.90
	78.60	151.80	16.15	29.82	14.30	29.90	14.60	29.00
	76.60	152.70	14.78	29.24	14.70	29.80	14.00	29.50
	75.10	151.80	14.98	28.85	14.50	29.10	14.70	28.80
	74.00	153.80	14.98	29.24	12.90	30.00	12.60	28.60
	78.40	155.00	16.54	30.02	14.20	30.70	12.10	28.80
	74.70	154.90	14.78	29.63	15.00	30.50	14.80	29.50
	73.30	154.20	14.00	29.82	11.10	30.00	9.50	29.50
	75.00	155.10	14.98	30.61	14.60	30.70	14.50	29.50
	77.00	153.30	14.98	30.00	14.40	29.00	12.60	27.70
	74.00	153.80	14.59	30.02	11.10	29.50	8.60	28.80
	77.10	151.60	16.74	29.24	15.50	29.00	15.10	27.90
	75.90	154.40	14.78	30.41	14.70	29.80	14.30	28.30
	74.00	153.00	15.37	29.24	13.00	29.40	11.00	28.00
	74.00	153.60	14.78	29.24	14.70	29.10	14.50	25.70
	76.10	154.20	14.78	29.63	14.40	28.60	12.70	25.60
	77.30	154.80	15.37	30.41	12.00	29.50	10.80	27.50
	77.20	154.30	15.95	30.02	11.20	29.40	9.00	26.20
	77.40	154.30	14.98	29.63	13.90	29.40	11.70	26.10
	82.50	155.30	16.15	30.22	15.40	29.90	15.50	26.60
	75.40	153.40	15.37	30.41	15.00	29.40	15.00	26.30
	77.30	154.40	15.95	30.60	11.00	29.60	8.90	26.10
	75.20	155.10	14.39	30.20	15.50	28.40	15.00	26.20
	75.80	153.40	14.78	30.41	11.30	28.30	8.70	27.10
	76.30	154.20	14.78	30.20	16.00	27.60	15.20	25.40
	75.60	154.30	15.95	29.20	11.30	27.50	10.00	25.50
	75.60	154.70	14.78	30.41	15.50	27.20	14.90	23.60
	76.10	155.40	15.17	30.02	15.60	28.00	15.30	25.20
$\overline{x}$	76.11	153.97	15.21	29.76	13.78	28.82	12.70	26.97
σ	2.03	1.34	0.67	0.60	1.63	1.62	2.37	1.86
CV	2.66 %	0.87 %	4.38 %	2.01 %	11.85 %	5.64 %	18.68 %	6.91 %

lowest standard deviation among all acceleration meters, even though the average peak acceleration value for MEMS was the highest. The acceleration recorded by piezoelectric accelerometers is characterized by the largest data spread. At the same time, the spread of data for piezoelectric accelerometers is significant, and for the 352C33 sensor, the coefficient of variation reaches almost 20 %. This is caused by the frequent repetition for this dataset of measured values that are much smaller than the others and much smaller than the values recorded by the MEMS accelerometer. The average value measured by the 352C33 sensor is 12.70 g, with results as low

as less than 9 g being repeated among the recorded data, i.e., values that are far from the average value by more than the standard deviation. For hammer impacts released at a pendulum swing angle of 40°, the values recorded by all sensors increased in proportion to the increase in the value of the pendulum swing angle. The spread of data between successive measurement systems exhibits analogous characteristics to those observed at 20°. Again, the lowest coefficient of variation is characterized by the data set recorded by the force sensor (less than 1 %), and a comparable level of spread is observed for MEMS (slightly above 2 %). As for the first dataset, the greatest spread in the data is characterized by the results recorded by piezoelectric accelerometers. However, for measurements at a pendulum swing angle of 40°, the recorded spread is much smaller and for piezoelectric accelerometers does not exceed 7 %. The decrease in spread for all measurement systems at impacts for a pendulum swing angle of 40° is most likely due to the fact that, for this case, we observe a larger change in the measured value, which makes it easier to register by the used measurement systems. In order to better show the spread of the data for the individual accelerometers, Fig. 8 shows box plots for impacts with pendulum swing angles of 20° and 40°.

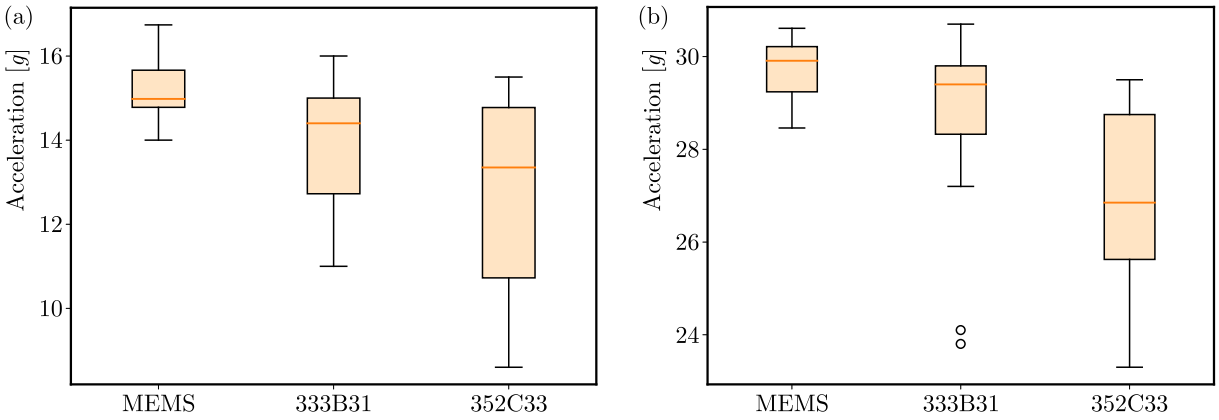

Fig. 8. Box plot showing the comparison of the measurement results of individual devices at impact for: (a) 20°; (b) 40°.

Box plots provide a graphical representation of the features of the data sets being ranked. Based on the box plots shown, it can be seen that the values recorded for the MEMS accelerometer are higher than for the other sensors, as evidenced by the median value, which is highest for the MEMS sensor. The difference in magnitude is most likely due to the fact that the recorder using the MEMS accelerometer records the data at the highest sampling rate, which significantly increases the chances of recording key points during the course of the impact. It can be seen that in all graphs the median is shifted relative to the center of the corresponding box plots, which indicates the asymmetry of the recorded data. In order to provide a more accurate illustration of the characteristics of the recorded data distributions, Figs. 9 and 10 present histograms for the data that was recorded at 20° and 40°, respectively.

As illustrated in the histograms, the normal distribution curve has been superimposed for the purpose of evaluating the resulting distributions, with the said curve having been drawn for the corresponding data sets based on their mean and standard deviation. The graphs presented in Fig. 9 show the asymmetric nature of the distribution for all measuring instruments. However, for the FC500 force sensor and for the MEMS accelerometer, the data sets manifest some characteristics of a normal distribution, and it can be assumed that with an increase in the measurement sample, the results for these sensors could be estimated with the help of a normal distribution. However, the results for piezoelectric accelerometers are characterized by a large asymmetry. Furthermore, a high frequency of occurrences is observed in the upper and lower extreme intervals of the histogram. This is an unexpected result for this type of measurement, and it is not recorded by other measurement systems. This is most likely related to the frequent failure of piezoelectric sensors to register the maximum value in the peak. This

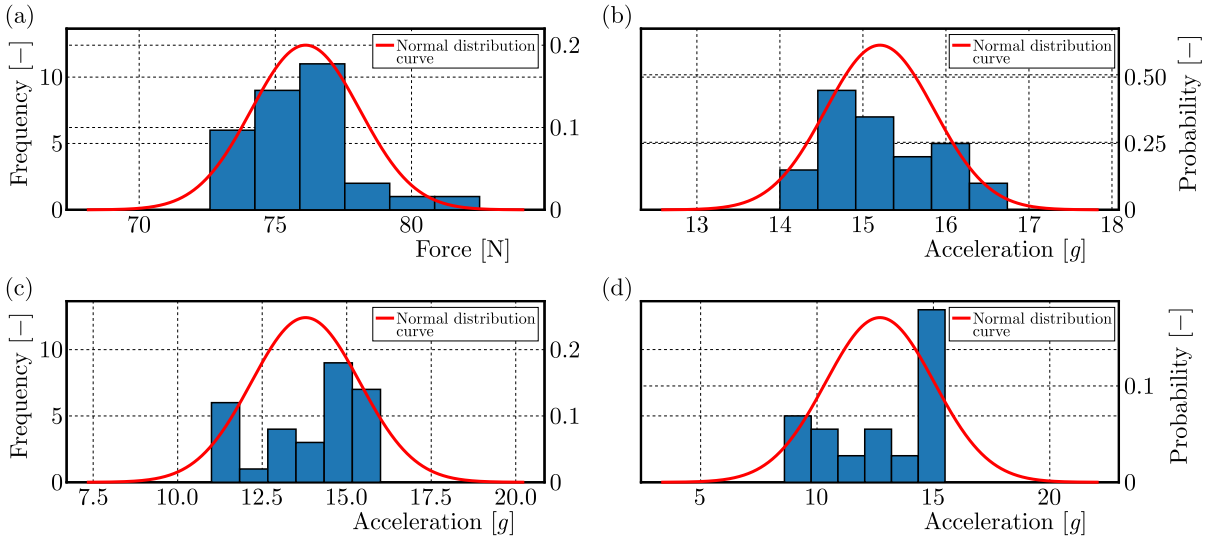

Fig. 9. Histograms showing the distribution of measurement results for different devices with a normal distribution curve determined from the sample mean and standard deviation at impact for 20°. Histograms are shown successively for: (a) FC500 force sensor; (b) MEMS-type accelerometer; (c) 333B31 piezoelectric sensor; (d) 352C33 piezoelectric sensor.

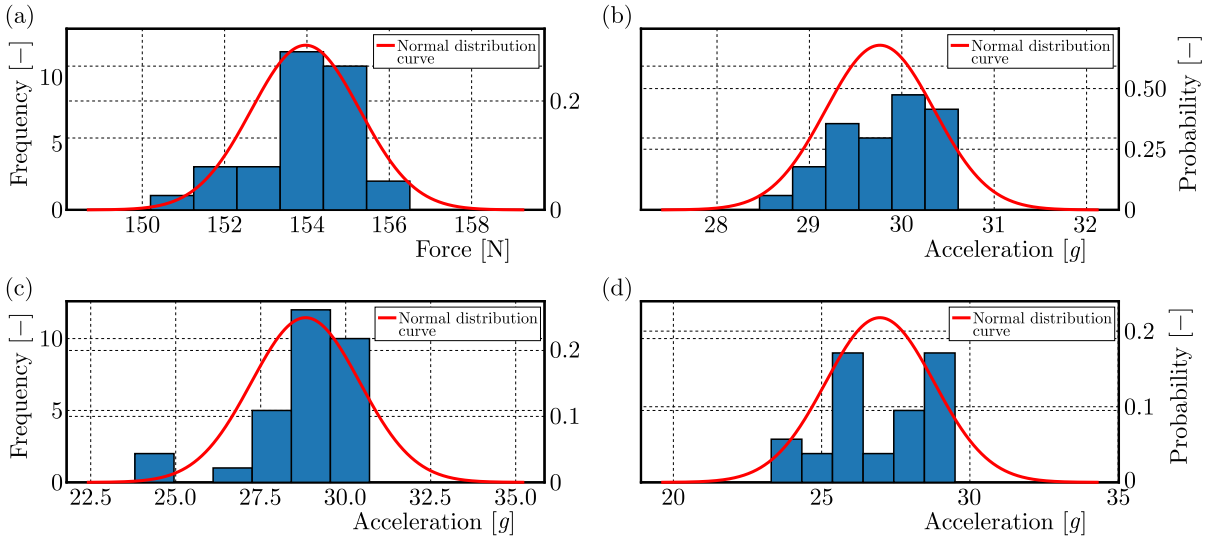

Fig. 10. Histograms showing the distribution of measurement results for different devices with a normal distribution curve determined from the sample mean and standard deviation at impact for 40°. Histograms are shown successively for: (a) FC500 force sensor; (b) MEMS-type accelerometer; (c) 333B31 piezoelectric sensor; (d) 352C33 piezoelectric sensor.

leads to registering, for the maximum acceleration value, the value occurring before or after the maximum value in the peak, and therefore, registering a smaller value than the actual value.

The distribution of rasterized data for an impact at a pendulum deflection angle of 40° is analogous to that for 20°. It is important to note that the data recorded by the 333B31 sensor is an exception to this. Indeed, for this particular angle, the data shows the characteristics of a normal distribution to a higher degree. However, it is also important to note that significant outliers are observed here, as evidenced by a break in the continuity of the histogram. In the histograms, individual results can be observed that significantly deviate from the other measured values (which is particularly evident for the 333B31 piezoelectric accelerometer). If the purpose of the conducted research was to determine acceleration values, these results should be discarded.

However, the purpose of the conducted research is to compare different measurement methods. The frequency of occurrence of this type of interference is an important element from the point of view of this comparison. In addition, it testifies in favor of the assumption that for piezoelectric accelerometers, the observed inaccuracies are the result of not recording the maximum value of acceleration in the peak.

Also important from the point of view of evaluating the characteristics of the shock wave is the quality of recording the acceleration waveform. To visualize this, Fig. 11 shows the acceleration waveform during the impact of the hammer with a pendulum swing of 20°.

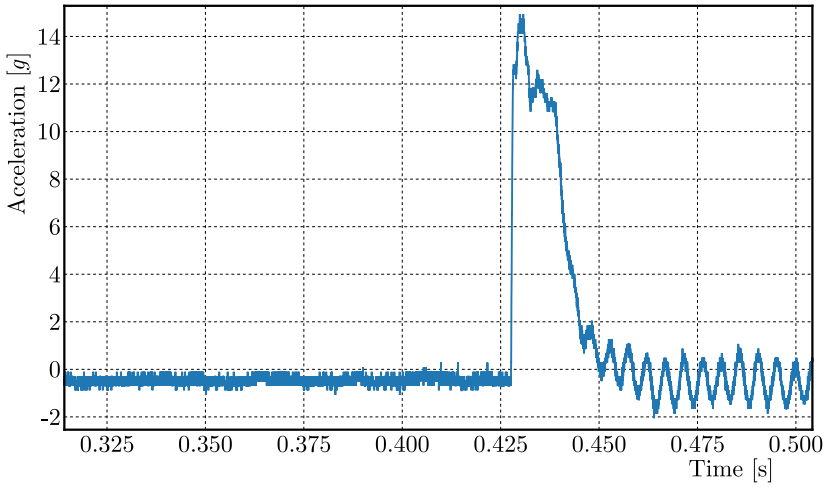

Fig. 11. Waveform of acceleration during the impact of the hammer at a pendulum deflection of 20°.

It can be observed that the authors' data logger managed to record the acceleration peak occurring during the hammer impact to a degree that allowed determining the maximum value and also determining the time of impact. In addition, using the MEMS accelerometer, it was also possible to record vibrations occurring in the system immediately after the hammer impact, which is visible in the form of a harmonic acceleration course visible immediately after the impact.

4. Conclusions

As a result of the conducted research, it can be concluded that the use of a system based on the SPI protocol with a MEMS sensor allows precise and repeatable results to be obtained in various dynamic applications. Comparison of the results with the piezoelectric sensor system based on force sensors and piezoelectric accelerometers confirms the consistency of measurements and the effectiveness of using MEMS in the analysis of dynamic phenomena.

Conclusions:

- universality of the SPI system: the system based on the SPI protocol with a MEMS sensor provides flexibility and wide application possibilities in dynamic measurements;
- wider frequency range: the SPI system with MEMS works correctly up to 45 kHz, which gives an advantage over traditional piezoelectric sensor systems that only work up to 20 kHz;
- repeatability of measurements: the system demonstrates high repeatability of results and low scatter, which confirms the reliability of the MEMS sensor in measurements;
- compatibility with piezoelectric sensors system: the results obtained from the MEMS sensor-based SPI system are consistent with those of the piezoelectric sensors system, which demonstrates its precision.

References

1. ADXL377. Retrieved January 10, 2025, from: https://www.analog.com/en/products/adxl377.html
2. Anand, N., Joseph, G., Oommen, S.S., & Dhanabal, R. (2014). Design and implementation of a high speed Serial Peripheral Interface. *2014 International Conference on Advances in Electrical Engineering (ICAEE). IEEE.* https://doi.org/10.1109/ICAEE.2014.6838431
3. Arkusz, K., Klekiel, T., Sławiński, G., & Będziński, R. (2019). Influence of energy absorbers on Malgaigne fracture mechanism in lumbar-pelvic system under vertical impact load. *Computer Methods in Biomechanics and Biomedical Engineering*, *22*(3), 313–323. https://doi.org/10.1080/10255842.2018.1553238
4. Baranowski, P., Małachowski, J., & Mazurkiewicz, Ł. (2020). Local blast wave interaction with tire structure. *Defence Technology*, *16*(3), 520–529. https://doi.org/10.1016/j.dt.2019.07.021
5. Brezeanu, I.B., Botezatu, C., Drăghici, F., & Brezeanu, G. (2022). Improved SPI controlled, low-voltage, high speed, multi-channel switch. *2022 14th International Conference on Electronics, Computers and Artificial Intelligence (ECAI). IEEE.* https://doi.org/10.1109/ECAI54874.2022.9847444
6. Coşkun, O., Egeli, E., Tarcan, E., Kurtuluş, İ., & Yılmaz, G. (2023). Analysis and implementation of a daisy-chain serial peripheral interface bus for a communication network with multiple PLC modules. *2023 14th International Conference on Electrical and Electronics Engineering (ELECO). IEEE.* https://doi.org/10.1109/ELECO60389.2023.10416045
7. Covaciu, D., & Dima, D.S. (2017). Crash tests data acquisition and processing. In A. Chiru, & N. Ispas (Eds.), *CONAT 2016 International Congress of Automotive and Transport Engineering* (pp. 782–789). Springer, Cham. https://doi.org/10.1007/978-3-319-45447-4_85
8. Dima, D.S., & Covaciu, D. (2017). Solutions for acceleration measurement in vehicle crash tests. *IOP Conference Series: Materials Science and Engineering*, *252*, Article 012007. https://doi.org/10.1088/1757-899X/252/1/012007
9. Elsayed, N.M., & Atkins, J.L. (Eds.). (2008). *Explosion and blast-related injuries: Effects of explosion and blast from military operations and acts of terrorism.* Elsevier Academic Press.
10. Erdik, A., Kilic, S.A., Kilic, N., & Bedir, S. (2016). Erratum to: Numerical simulation of armored vehicles subjected to undercarriage landmine blasts (Shock Waves, 10.1007/s00193-015-0576-1). *Shock Waves*, *26*(4), 531. https://doi.org/10.1007/s00193-016-0678-4
11. FC500. Retrieved January 10, 2025, from: https://www.axis.pl/en/fc/405-fc500.html
12. Kciuk, M., Kowalik, Z., Lo Sciuto, G., Sławski, S., & Mastrostefano, S. (2023). Intelligent medical velostat pressure sensor mat based on artificial neural network and Arduino embedded system. *Applied System Innovation*, *6*(5), Article 84. https://doi.org/10.3390/asi6050084
13. Kciuk, S., Krzystała, E., Mężyk, A., & Szmidt, P. (2022). The application of microelectromechanical systems (MEMS) accelerometers to the assessment of blast threat to armored vehicle crew. *Sensors*, *22*(1), Article 316. https://doi.org/10.3390/s22010316
14. Lynch, K.M., Marchuk, N., & Elwin, M.L. (2015). *Embedded computing and mechatronics with the PIC32 microcontroller.* Newnes.
15. Mohd Noor, N.B., & Saparon, A. (2012). FPGA implementation of high speed serial peripheral interface for motion controller. *2012 IEEE Symposium on Industrial Electronics and Applications.* IEEE. https://doi.org/10.1109/ISIEA.2012.6496676
16. Olvey, S.E., Knox, T., & Cohn, K.A. (2004). The development of a method to measure head acceleration and motion in high-impact crashes. *Neurosurgery*, *54*(3), 672–677. https://doi.org/10.1227/01.NEU.0000108782.68099.29
17. Park, J., & Mackay, S. (2003). Appendix F – Number systems. In *Practical Data Acquisition for Instrumentation and Control Systems* (pp. 389–397). Elsevier. https://doi.org/10.1016/B978-075065796-9/50018-5

18. Pyka, D., Kurzawa, A., Żochowski, P., Bajkowski, M., Magier, M., Grygoruk, R., Roszak, M., Jamroziak, K., & Bocian, M. (2025). Experimental and numerical research on additional vehicles protection against explosives. *Archives of Civil and Mechanical Engineering*, *25*(2), Article 83. https://doi.org/10.1007/s43452-025-01121-w

19. Sethuramalingam, T.K., & Vimalajuliet, A. (2010). Design of MEMS based capacitive accelerometer. *2010 International Conference on Mechanical and Electrical Technology*. IEEE. https://doi.org/10.1109/ICMET.2010.5598424

20. Texas Instruments (2010, rev. 2019). KeyStone Architecture Serial RapidIO (SRIO). User's Guide. https://www.ti.com/lit/ug/sprugw1c/sprugw1c.pdf

21. Vijaya, V., Valupadasu, R., Chunduri, B.R., Rekha, C.K., & Sreedevi, B. (2011). FPGA implementation of RS232 to Universal serial bus converter. *2011 IEEE Symposium on Computers and Informatics*. IEEE. https://doi.org/10.1109/ISCI.2011.5958920

22. Wrazidło, D., Sławski, S., Krzystała, E., & Jarosz, T. (2025). Numerical analysis of shock wave impact on a gas cylinder. In E. Świtoński, A. Mężyk, S. Kciuk, & R. Szewczyk (Eds.), *Lecture Notes in Networks and Systems: Vol. 1146. PCM—CMM2023: Theories, Models and Simulations of Complex Physical Systems* (pp. 196–207). Springer. https://doi.org/10.1007/978-3-031-73161-7_18

23. 333B31. Retrieved January 10, 2025, from: https://www.pcb.com/products?m=333b31

24. 352C33. Retrieved January 10, 2025, from: https://www.pcb.com/products?m=352c33

Manuscript received May 5, 2025; accepted for publication June 18, 2025; published online October 7, 2025.